




**Charge density wave transition in the magnetic topological semimetal EuAl<sub>4</sub>**R. Yang <sup>1,2,\*</sup>, C.-C. Le,<sup>3,\*</sup> P. Zhu,<sup>4,5</sup> Z.-W. Wang,<sup>4,5,6,†</sup> T. Shang,<sup>7</sup> Y.-M. Dai,<sup>8,9,‡</sup> J.-P. Hu <sup>10</sup> and M. Dressel <sup>2,§</sup><sup>1</sup>Key Laboratory of Quantum Materials and Devices of Ministry of Education, School of Physics, Southeast University, Nanjing 211189, China<sup>2</sup>1. Physikalisches Institut Universität Stuttgart, 70569 Stuttgart, Germany<sup>3</sup>RIKEN Interdisciplinary Theoretical and Mathematical Sciences (iTHEMS), Wako, Saitama 351-0198, Japan<sup>4</sup>Centre for Quantum Physics, Key Laboratory of Advanced Optoelectronic Quantum Architecture and Measurement (MOE), School of Physics, Beijing Institute of Technology, Beijing 100081, China<sup>5</sup>Beijing Key Lab of Nanophotonics and Ultrafine Optoelectronic Systems, Beijing Institute of Technology, Beijing 100081, People's Republic of China<sup>6</sup>Material Science Center, Yangtze Delta Region Academy of Beijing Institute of Technology, Jiaxing 314011, People's Republic of China<sup>7</sup>Key Laboratory of Polar Materials and Devices (MOE), School of Physics and Electronic Science, East China Normal University, Shanghai 200241, China<sup>8</sup>National Laboratory of Solid State Microstructures and Department of Physics, Nanjing University, Nanjing 210093, China<sup>9</sup>Collaborative Innovation Center of Advanced Microstructures, Nanjing University, Nanjing 210093, China<sup>10</sup>Institute of Physics, Chinese Academy of Sciences, Beijing 100190, China

(Received 28 April 2023; revised 11 January 2024; accepted 12 January 2024; published 30 January 2024)

In rare-earth intermetallic topological materials, carriers from topological bands mediate the magnetic interactions between local moments, giving rise to a plethora of exotic quantum phenomena. Recently, anomalous magnetic instability, helical spin orders, and skyrmions were found in topological semimetal EuAl<sub>4</sub> with tetragonal lattice. Comparing with its counterpart EuGa<sub>4</sub>, which does not show intricate magnetism, the difference lies in the presence of charge-density wave (CDW) order in EuAl<sub>4</sub>. Thus, studying the effect of CDW transition on electronic structure is decisive for the final understanding of the intricate magnetism in topological materials. Here, we studied the charge excitations in EuAl<sub>4</sub> across the CDW transition through optical spectroscopy and the first-principles calculations. After the CDW transition, a partial gap (60 meV) on the Fermi surface and an enhanced mid-infrared absorption at around 0.4 eV were observed in the optical conductivity. With the magneto-optical spectroscopy, we further observed the evolution of charge excitations alongside the magnetization. Through the first-principles calculations, we have identified that the CDW transition not only partially erodes the Fermi surface contributed by the topological bands but also modulates the high-energy excitations between the bands dominated by Eu 5*d* and Al 3*p* orbitals. In the counterpart EuGa<sub>4</sub>, the band reconstruction is absent. Since the itinerant carriers and *pd* hybridizations are usually assigned to mediate the magnetic interactions, our findings offer unprecedented insights to understanding the complex magnetism observed in highly symmetric topological semimetals.

DOI: [10.1103/PhysRevB.109.L041113](https://doi.org/10.1103/PhysRevB.109.L041113)

**Introduction.** Interactions between topology, many-body effects, and magnetism represent one of the research frontiers in condensed matter physics [1–4]. Topology coupling with the charge-density wave (CDW) can give rise to an axion insulator state [5], while the entanglement of magnetism and topology leads to intriguing phenomena such as quantum anomalous Hall effects and skyrmions [3,6]. However, the interplay between topology, magnetism, and CDW in one system remains largely unexplored. Rare-earth intermetallic compounds, in which the local moments of rare-earth atoms interact with the itinerant carriers from topological bands, provide an ideal platform for studying and manipulating novel

topological physics [7–11]. Recently, the CDW transition and chiral spin textures including skyrmions were observed concomitantly in a group of rare-earth magnetic topological semimetals with highly symmetric tetragonal lattices [12–16]. These phenomena are unexpected, and despite a number of investigations [12,14,16–19], the underlying mechanism remains controversial. Given that charge excitations mediate the magnetic interactions, unraveling the modulation of band structure by the CDW order will provide a pivotal clue for resolving this issue.

The binary compounds EuM<sub>4</sub> (M = Al, Ga) family provides an unique arena for investigating the intricate interplay between CDW, topology, and magnetism due to their stoichiometric composition and relatively simple band and lattice structures (*I4/mmm*) [12,13,20]. In EuM<sub>4</sub>, magnetism originates from the local 4*f* electrons of Eu<sup>2+</sup> atoms that are sandwiched between M<sub>4</sub> layers. The magnetic interactions are mediated either by itinerant carriers in M<sub>4</sub> layers through

\*These authors contributed equally to this work.

†zhiweiwang@bit.edu.cn

‡ymdai@nju.edu.cn

§dressel@pi1.physik.uni-stuttgart.de

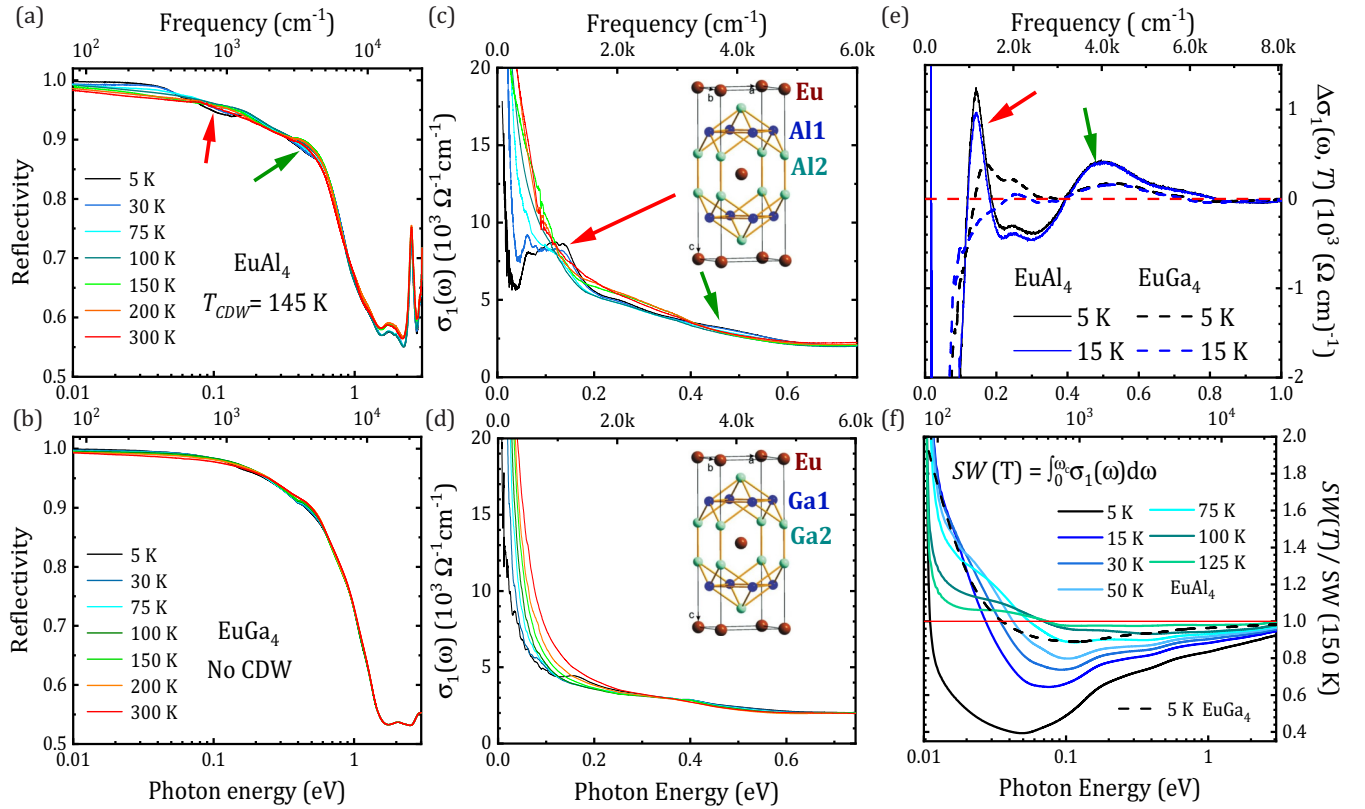


FIG. 1. Optical spectroscopy of  $\text{EuAl}_4$  and  $\text{EuGa}_4$ . Temperature-dependent reflectivity of (a)  $\text{EuAl}_4$  and (b)  $\text{EuGa}_4$  from 80 to 24 000  $\text{cm}^{-1}$  with the light polarized in the  $ab$  plane. In panel (a), the reflectivity changes in  $\text{EuAl}_4$  below  $T_{\text{CDW}} = 145$  K are highlighted by red and green arrows. (c)–(d) Temperature evolution of the real part  $\sigma_1(\omega; T)$  of the optical conductivity spectra of (c)  $\text{EuAl}_4$  and (d)  $\text{EuGa}_4$  below 6000  $\text{cm}^{-1}$  (0.74 eV); the emergent absorption features after the CDW transition are indicated by red and green arrows in panel (c). The insets display the lattice structure of  $\text{EuAl}_4$  and  $\text{EuGa}_4$ , which contain two inequivalent Al/Ga atoms. (e) Difference spectra of  $\sigma_1(\omega)$  below the CDW transition calculated through  $\Delta\sigma_1(\omega, T) = \sigma_1(\omega, T) - \sigma_1(\omega, 150 \text{ K})$ . The newly developed absorption is indicated by the colored arrows. The solid and dashed lines represent the  $\text{EuAl}_4$  and  $\text{EuGa}_4$  data, respectively. (f) The integrated spectral weight ( $SW$ ) of  $\text{EuAl}_4$  according to Eq. (1), normalized by the  $SW$  at  $T = 150$  K, is plotted for  $T < T_{\text{CDW}}$  as a function of the cutoff frequency  $\omega_c$ ; the  $SW$  redistribution takes place in a broad energy range.

Ruderman-Kittel-Kasuya-Yosida (RKKY) interaction (antiferromagnetic, AFM) or by local excitations (ferromagnetic, FM), thus the band structure plays a crucial role in determining the magnetic ground state at low temperatures ( $T$ 's) [21]. For  $\text{EuAl}_4$ , a CDW transition occurs at  $T_{\text{CDW}} = 145$  K and a consecutive of intricate magnetic orders with noncoplanar spin textures forming below 15.6 K [22]. The magnetism in  $\text{EuAl}_4$  is highly susceptible and can be easily disrupted by a weak magnetic field ( $< 2$  T), resulting in unexpected helical spin order and skyrmions in such centrosymmetric lattice [12]. In contrast, the counterpart  $\text{EuGa}_4$ , which lacks CDW, exhibits a highly stable collinear A-type AFM magnetic order up to 7 T [23]. Given that  $\text{EuAl}_4$  and  $\text{EuGa}_4$  have the same lattice structure and similar band structures [21], it is evident that the presence of CDW order plays a decisive role in influencing the magnetism of  $\text{EuAl}_4$ . Previous studies on both  $\text{EuAl}_4$  [24] and  $\text{EuGa}_4$  [25] have observed Dirac nodal lines near the Fermi level contributing to itinerant carriers that mediate the magnetic interactions. Furthermore, recent experimental [13,20] and theoretical [26,27] investigations indicated a small nesting vector connecting the Dirac-like bands and considerable electron-phonon coupling in  $\text{EuAl}_4$ . Nevertheless, the nature of the CDW gap as well as the impact

of CDW order on band structures continue to elude us, for the lack of precise observations.

Optical spectroscopy is the superior method for studying charge excitations between different bands, providing information of gaps and band reconstructions [28–31]. In this work, we conducted a comparative investigation between  $\text{EuAl}_4$  and  $\text{EuGa}_4$  to elucidate the effects induced by CDW transition on electronic structure by means of the optical spectroscopy and the first-principles calculations. In optical spectroscopy, we first observed the CDW gap (60 meV) in  $\text{EuAl}_4$  below  $T_{\text{CDW}}$ . The CDW order not only partially eliminates the Fermi surface but also affects the high-energy excitations at around 0.4 eV, which is further enhanced by external field. With the first-principles calculations, we identified the band reconstruction induced by the CDW transition and further discussed its potential impact on the magnetism of  $\text{EuAl}_4$ .

#### Results.

*Optical spectroscopy.* Figures 1(a) and 1(b) display  $\text{EuAl}_4$ 's and  $\text{EuGa}_4$ 's temperature ( $T$ )-dependent reflectivity  $R(\omega)$  spanning from the far-infrared (FIR) to ultraviolet range, respectively; details of the measurements are described in Sec. II of the Supplemental Material (SM) [32]. The high

reflectivities ( $>0.9$ ) that gradually increase with decreasing  $T$  and a pronounced plasma edge around 0.9 eV evidence their metallic nature. When  $T < T_{\text{CDW}}$ ,  $\text{EuAl}_4$ 's  $R(\omega)$  is suppressed around 0.1 (red arrow), 0.5 (green arrow), and 1.5 eV, indicating emergent absorptions after the CDW transition [28,29,31], while no additional structure develops in  $\text{EuGa}_4$ 's  $R(\omega)$  from 300 to 5 K.

Based on the Kramers-Kronig analysis, the optical conductivity was derived from  $R(\omega)$  (see detail in Sec. II of the SM [32]). For both compounds, the optical conductivities are plotted in Figs. 1(c) and 1(d), respectively. The real part of the optical conductivity  $\sigma_1(\omega)$ , which reflects the joint density of states [28], displays intraband zero-energy modes (Drude peak) that roll off with a characteristic width, which represents the scattering of itinerant carriers. With increasing photon energy, the Drude peaks gradually develop into a series of interband absorptions (Lorentz peaks). Across the CDW transition, in  $\text{EuAl}_4$ 's  $\sigma_1(\omega)$  [Fig. 1(c)], we encounter a great depletion of intraband responses with emergent absorption peaks around 0.1 and 0.4 eV, signaling the formation of CDW gap on the Fermi surface and a band reconstruction at high-energy range [29,31]. Since the intraband responses persist to 5 K, the Fermi surface is only partially gapped. At 5 K, the newly formed absorptions around 0.1 eV evolve into a plateaulike structure, which cannot be ascribed to a single Lorentz peak. In contrast, without the CDW transition,  $\text{EuGa}_4$ 's  $\sigma_1(\omega)$  is remarkably different: only a continuously narrowing Drude peak, which reflects diminishing scattering rate upon cooling, is observed down to 15 K [Fig. 1(c)]. When entering into the AFM state, with greatly suppressed spin fluctuations, the Drude peak exhibits a remarkable narrowing and a small bump emerges at 0.17 eV.

In Fig. 1(e), the difference spectra  $\Delta\sigma_1(\omega)$  respect to 150 K were calculated for both samples. They further show affections caused by the CDW transition [33,34]. For  $\text{EuAl}_4$ , the negative  $\Delta\sigma_1(\omega)$  at low energy range and two remarkable absorption peaks around 0.1 (red arrow) and 0.4 eV (green arrow) deliver the message that besides the partial gap on the Fermi surface, the high-energy excitations are also affected (green arrow). However, the changes in  $\text{EuGa}_4$ 's  $\sigma_1(\omega)$  above 0.1 eV are not that dramatic and mainly come from the temperature effects (e.g., narrowing of the absorption peaks).

To elucidate the spectral weight ( $SW$ ) redistribution caused by the CDW transition in  $\text{EuAl}_4$ , we calculated the integrated  $SW$  of the measured  $\sigma_1(\omega)$  up to the cutoff frequency ( $\omega_c$ ), which is given by [28,35]

$$SW(\omega_c; T) = \frac{Z_0}{\pi} \int_0^{\omega_c} \sigma_1(\omega'; T) d\omega', \quad (1)$$

expressed in units of  $\text{cm}^{-2}$  ( $Z_0 = 377 \Omega$  being the impedance of vacuum). Such model-independent value is related to the carriers (normalized to their effective mass) contributing to the optical excitations up to  $\omega_c$  and reflects the evolution of the band structures at various temperatures. In the limit  $\omega \rightarrow \infty$ , the  $SW$  is expected to converge to a constant value, satisfying the optical  $f$ -sum rule [28]. To show the affection from CDW transition, we calculate the ratio  $SW(\omega_c; T)/SW(\omega_c; 150 \text{ K})$ , which underscore the energy range of the  $SW$  reshuffling as a function of  $T$  with respect to 150 K, which is slightly above  $T_{\text{CDW}}$  [36]. The results presented in Fig. 1(f) display

a twofold  $SW$  reshuffling to low and high energy ranges for both samples. In the low-energy range, the narrowing of the Drude peak gives rise to the accumulation of  $SW$  in a very small FIR energy range and a ratio above 1. In  $\text{EuAl}_4$ , the suppressed intraband responses caused by the opening of CDW gap result in a ratio  $SW(\omega_c; T)/SW(\omega_c; 150 \text{ K})$  far below 1, and its minimum corresponds to the energy scale of the single-particle gap excitation within the electronic structure, based on which the CDW gap is estimated to be 60 meV (5 K) [29]. Even though the  $SW$  starts to recover above the gap, it is not fully retrieved until 3 eV, which is the highest energy for our measurements, indicating a very broad energy range for the  $SW$  reshuffling. Such behavior has been widely observed in  $\text{LiV}_2\text{O}_4$  [37], iridates [38], and cuprates [39], reflecting a strong correlation effect, which is further confirmed by estimating the renormalization of electronic kinetic energy (see Sec. III of the SM [32]) [40]. Thus, the  $SW$  analysis also confirms the partial gap and the enhanced high-energy excitations after the CDW transition. Such tendency is additionally enhanced by the correlation effect. However, without the CDW order,  $\text{EuGa}_4$ 's  $SW$  is just marginally suppressed and shifted to very high-energy range [the black dashed line in Fig. 1(f)], primarily attributed to the correlation effect.

Drude(D)-Lorentz(L) fit to the optical conductivity. With the goal to quantitatively describe the electrodynamic responses across the CDW transition, the  $\sigma_1(\omega)$  of  $\text{EuAl}_4$  and  $\text{EuGa}_4$  were fit within the common Drude-Lorentz phenomenological approach (we refer to Sec. III of SM [32] for details of the fit). The resulting fits with their constituent components are displayed in Figs. 2(a) and 2(c) and Fig. S3 in the SM [32]. At high  $T$ 's, both samples'  $\sigma_1(\omega)$  can be described by two Drude (D) components with different widths (scattering rate) and the same number of Lorentzian (L) oscillators, signaling their similar band structures (see Fig. S3 and the discussion in Sec. III of the SM [32] for detail). After the CDW transition,  $\text{EuAl}_4$ 's two Drude components are significantly suppressed, giving way to a newly formed Lorentz peak around 60 meV originating from the CDW gap that partially opens on the Fermi surface, Fig. 2(a), while  $\text{EuGa}_4$  keeps robust intraband responses down to 5 K, Fig. 2(c). Through an analysis of the  $SW$  distribution of each intraband and interband response [the  $SW$  was defined as squared plasma frequency ( $\omega_{pD}^2$ ) or oscillator strength ( $\Omega_j^2$ ) of each fit component], we notice that in  $\text{EuAl}_4$ , above  $T_{\text{CDW}}$ , the  $SW$  of each component does not show discernible change, while in the CDW ordered state, the  $SW$  of intraband responses is significantly suppressed by almost 60% (5 K) and transferred to CDW absorptions, mid-infrared (MIR) interband transitions around 0.4 eV [Fig. 2(c)], and higher energy absorptions. In contrast, the  $SW$  of the MIR absorption in  $\text{EuGa}_4$  shows almost no  $T$  dependence [Fig. 2(d)], a marginal suppression of the Drude components can be attributed to the correlation effects.

*Magneto-optical spectroscopy.* Up to now, we have learned that, besides the CDW gap, the other difference between  $\text{EuAl}_4$  and  $\text{EuGa}_4$  is the enhanced MIR absorptions. To further trace the evolution of MIR absorptions under magnetic field, we measured the magneto-optical spectra with an *in situ* magnetic field along the  $c$  axis ( $H \parallel c$ ). The results shown in Fig. 3(a) exhibit no discernible change in reflectivity below 0.5 T. For  $H > 0.5$  T, the low-energy reflectance increases

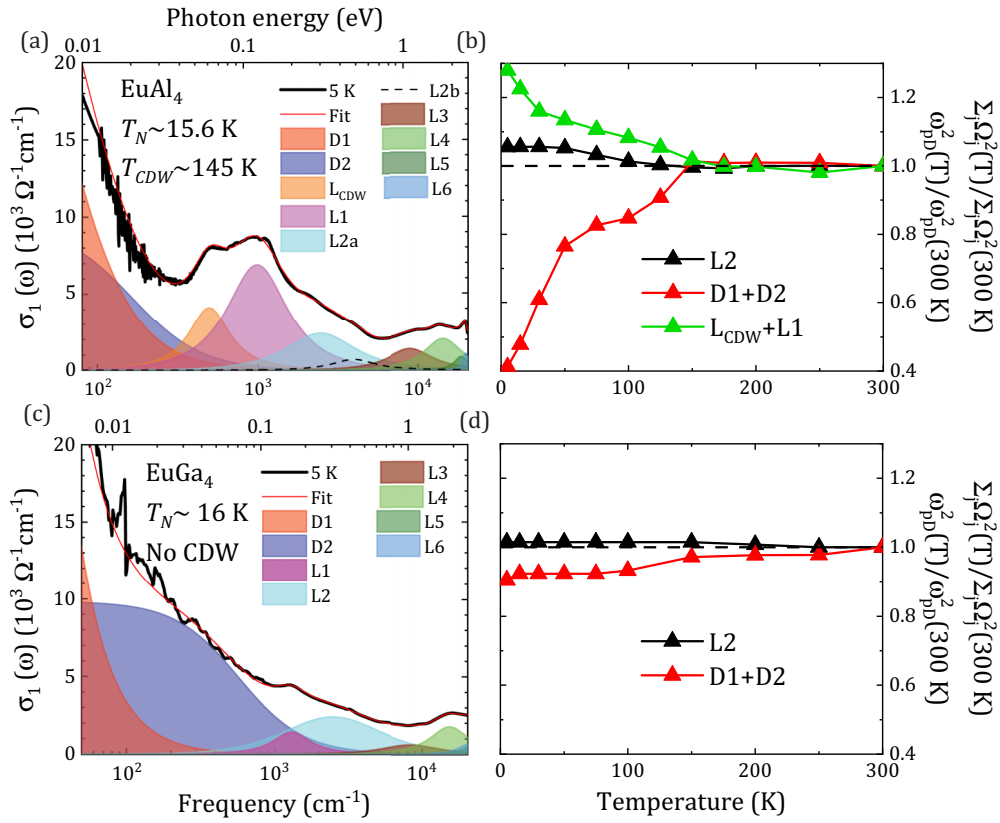


FIG. 2. Drude(D)-Lorentz(L) fit to the optical conductivity. The fits to  $\text{EuAl}_4$ 's (a) and  $\text{EuGa}_4$ 's (c) optical conductivity at 5 K; the optical conductivities can be decomposed into the narrow and broad Drude components, as well as several Lorentz oscillators. (b) and (d) are  $T$ -dependent spectral weight of the Drude components ( $\omega_{pd}^2 = \omega_{pd1}^2 + \omega_{pd2}^2$ ) and the Lorentz components ( $\sum_j \Omega_j^2$ ) normalized to the value at 300 K. Refer to Sec. III of the SM [32] for more details.

slightly but the reflectivity above 0.25 eV is suppressed continuously; this behavior saturates at 3 T. In  $T$ -dependent  $R(\omega)$  (Fig. 1(a) and Fig. S2(b) in the SM [32]), the suppression in reflectivity after the CDW transition stems from the absorptions of the CDW gap in the FIR range and enhanced MIR optical responses [41]; thus, in Fig. 3(b) we plot the change in reflectivity at 0.5 eV under magnetic field  $\Delta R(H, 0.5 \text{ eV})$  and

make a comparison with the magnetization  $M(H)$  [42]. Their similar field dependence indicates that the MIR absorptions in  $\text{EuAl}_4$  is further enhanced while aligning the local moments. On the other side, the slightly enhanced  $R(\omega)$  below 0.25 eV reflects the enhanced metallicity, which may come from the Zeeman effect transforming the Fermi surface (as shown in Fig. S6(a) in the SM [32]).

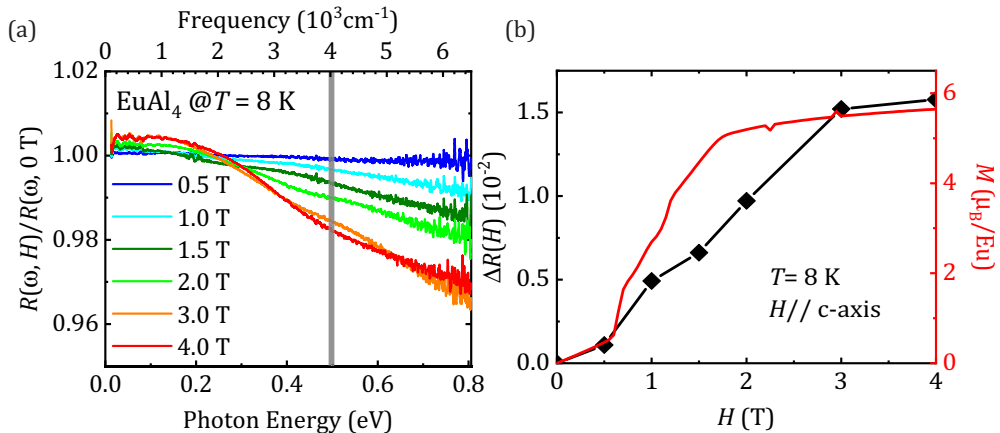


FIG. 3. Magneto-optical response of  $\text{EuAl}_4$ . (a) Magneto-optical reflectivity spectra  $R(\omega, H)$  measured under out-of-plane fields  $H$  from 0 to 4 T and normalized to the zero-field reflectivity  $R(\omega, 0 \text{ T})$ . (b) Comparison between the field-dependent reflectivity change  $\Delta R(H) = [1 - R(H)/R(0T)]$  at 0.5 eV [the gray bar in (a)] and the magnetization (red).

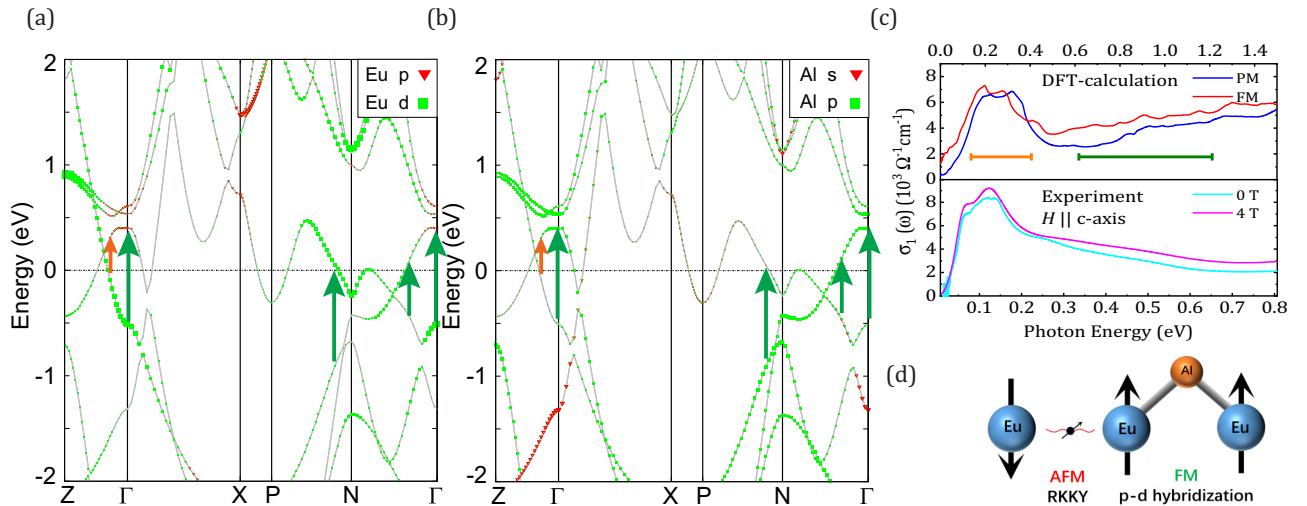


FIG. 4. The first-principles calculations. (a) and (b) display the band structures of EuAl<sub>4</sub> in PM state without the CDW order; the contribution from Eu 5*d* and Al 3*p* orbitals are highlighted in (a) and (b), separately. The upper and lower panels of (c) show the calculated and the measured interband optical conductivities. Blue and red lines in upper panel correspond to the absorptions in PM and FM (Eu's moments along the *c* axis) states, and turquoise and pink lines are conductivities measured at 8 K under external fields. Orange and green segments represent the interband transitions denoted by the same colored arrows in (a) and (b). (d) is the sketch of magnetic interactions in EuAl<sub>4</sub>.

**Band structure calculation.** Next we calculate the band structure and simulate the optical conductivity based on the density-functional theory (DFT) to get a better understanding to the changes in  $\sigma_1(\omega)$  across the CDW transition. The band structures in the paramagnetic (PM) state (without the CDW order) are shown in Figs. 4(a) and 4(b). At low energies, several bands cross the Fermi level giving rise to hole and electron pockets; along the  $\Gamma$ -Z direction of the Brillouin zone, two linear bands cross each other generating a Dirac cone, in line with the Dirac semimetal nature of EuAl<sub>4</sub>. From the perspective of orbital composition, the bands near the Fermi level are dominated by Eu 5*d* and Al 3*p* orbitals as illustrated by colors in Figs. 4(a) and 4(b). The overlap of these orbitals in several bands indicates considerable hybridizations between them [43].

The overall band-structure calculations lay the foundation for obtaining the interband components of the optical conductivity. Figure 4(c) displays the calculated  $\sigma_1(\omega)$  of EuAl<sub>4</sub> (upper panel) compared with the measured spectrum (lower panel) [44]. To mimic the magnetic field effect, in the upper panel, we calculated the  $\sigma_1(\omega)$  in both PM and field-forced FM states (the band structure with Eu moments along the *c* axis can be seen in Fig. S6(a) of the SM [32]). In the lower panel of Fig. 4(c), by fit the measured reflectivity, the interband  $\sigma_1(\omega)$  at 4 T, when the magnetic moments are fully aligned, was generated (see Sec. III of the SM [32] for detail). The similar lineshape and field dependency between theoretical and experimental results allows us to find good correspondences between them. The difference in energy is due to the band renormalization caused by the correlation effects which were not considered in the DFT calculations [45]. Even though the CDW transition opens a partial gap on the Fermi surface and affects the MIR absorptions, good correspondence between measurements and calculations indicates that the overall band structure is not drastically distorted, which is

supported by recent ARPES observations [24,25]. Considering the energy size and the possible excitations near the Fermi level, we can ascribe the low-energy absorptions [denoted by the orange segment in Fig. 4(c)] to the excitations on the Dirac cones along the  $\Gamma$ -Z direction in the Brillouin zone [orange arrows in Figs. 4(a) and 4(b)]. In the measurements, this low-energy peak mixes with the intraband responses at high *T*s [Figs. 1(c) and 1(d)]. In EuAl<sub>4</sub>, below  $T_{\text{CDW}}$ , the suppressed Drude components give way to the absorptions from Dirac bands, which finally forms a plateaulike structure in  $\sigma_1(\omega)$  together with excitations from the CDW gap at 5 K [Fig. 1(c)]. For EuGa<sub>4</sub>, without the CDW gap, this low-energy peak appears only below  $T_N \sim 16$  K, when the Drude peak narrows obviously for the diminishing spin fluctuations in magnetic ordered state [Fig. 1(d)]. On the other hand, the MIR responses [green segment in Fig. 4(c)] can be ascribed to the excitations between bands dominated by Eu 5*d* and Al 3*p* orbitals [green arrows in Figs. 4(a) and 4(b)]. When Eu's moments are aligned, both the measured and calculated  $\sigma_1(\omega)$  show remarkably enhanced MIR absorptions, while the changes of low-energy peaks are minor. Furthermore, in calculated  $\sigma_1(\omega)$  (Fig. S6(b) of SM [32]), we notice that only the conductivity from 0.4 to 1.4 eV shows remarkable change in the FM state. Thus, the measurements and the calculations indicate that the MIR absorptions mainly come from the excitations between the bands dominated by Eu 5*d* and Al 3*p* orbitals and are enhanced by either the CDW transition or external field.

**Discussion.** In EuAl<sub>4</sub>, the mechanism of CDW transition remains controversial. Despite the proposal of Fermi surface nesting, the experimental evidence for CDW gaps and band folding remains elusive [20,24], and the electron-phonon coupling was also proposed to play a decisive role [26]. Here, by comparing with the isostructural and isoelectronic EuGa<sub>4</sub>, our optical measurement first identified the CDW gap with the size around 60 meV. Recent transport measurements revealed

suppressed hole carriers after the CDW transition [46]. In the band structure [Fig. 4(a)], only the linear bands along  $\Gamma$ -Z direction contributes the hole pockets, thus, we infer that the CDW transition in  $\text{EuAl}_4$  partially erodes the Fermi surface from Dirac bands, which may originate from the imperfect nesting [26]. While, in  $\text{EuGa}_4$ , the upshift of valence band worsening the nesting and much weaker electron-phonon coupling [26] could be the plausible reasons for the absent CDW order.

Since electronic excitations play a crucial role in mediating magnetic interactions, the identification of band reconstruction provides valuable clues to understanding the impact on magnetism following the CDW transition. In  $\text{EuM}_4$  family, the itinerant carriers deliver the RKKY AFM interactions between Eu's local moments from  $4f$  orbitals [Fig. 4(d)]. However, in  $\text{EuAl}_4$ , since the CDW transition eliminates part of the Fermi surface, with less carriers, the AFM interactions would be suppressed [12,20,27]. On the other side, the enhanced MIR absorptions around 0.4 eV after the CDW transition signals the enhanced excitations between the bands dominated by Eu  $5d$  and Al  $3p$  orbitals [Fig. 4(d)]. Since Eu  $5d$  orbitals are less than half-filling, the  $pd$  hybridization along the  $c$  axis was designated as the bridge delivering FM exchange interactions [19,47–49]. The CDW transition within the  $\text{Al}_4^{2-}$  layers changes the distance between Eu and Al atoms [20,50], thereby affecting the overlap between  $pd$  orbitals that delivers the FM interactions. Although optical data fall short of providing substantial evidence of enhanced FM response in  $\text{EuAl}_4$ , at low  $T$ 's, recent nuclear magnetic resonance and muon spin resonance measurement revealed vigorous out-of-plane FM fluctuations [51,52]. Under the out-of-plane field, magnetostriction measurements of  $\text{EuAl}_4$  revealed shrinking  $c$  axis under magnetic field [53]. With shorter interatom distance, larger overlap strengthens the hopping between Eu  $5d$  and Al  $3p$  orbitals, which could be one reason for the field-enhanced MIR absorptions. Given that the CDW modulation is primarily along the  $c$  axis [21], we propose that, by affecting the band structure, the CDW transition in  $\text{EuAl}_4$  could weaken the AFM interactions but strengthen the FM ones in the same direction. Considering the FM in-plane coupling, the CDW transition would lower the magnetocrystalline anisotropy [54]. In addition, with approaching AFM and FM interactions, their competition would also destabilize the magnetism, facilitating the spin flip under external field [21,38,53]. In contrast, for the counterpart  $\text{EuGa}_4$ , without the band reconstruction induced by CDW order, larger and intact Fermi surfaces give rise to collinear A-type AFM order with in-plane spin configuration, which is robust under magnetic field up to 7 T (refer to Sec. III of the SM [32] for detail) [13,23].

Moreover, since the CDW gap is partially opened on the Fermi surface, the AFM interactions mediated by itinerant

carriers will become anisotropic. The incommensurate lattice distortion below  $T_{\text{CDW}}$  breaks the inversion symmetry [20,50], which may split the Dirac band into the Weyl ones [8,26]. In such an anisotropic environment, it is possible for carriers from the Weyl bands to mediate anisotropic magnetic interactions that facilitate the formation of chiral spin textures [12,27,55]. Nevertheless, further experimental investigations are needed to validate this procedure.

*Conclusion.* In conclusion, to reveal the impact of the CDW order on  $\text{EuAl}_4$ 's band structure, we carried out comparative study of isostructural  $\text{EuAl}_4$  and  $\text{EuGa}_4$  through optical spectroscopy and the first-principles calculations. In the optical spectroscopy, we observed that the CDW transition opened a partial gap with the size of 60 meV on the Fermi surface and enhanced a MIR absorption at around 0.4 eV; the latter are further enhanced by external field. With the help of the first-principles calculations, we identify that the CDW transition partially erodes the Fermi surface from the topological bands but enhances the excitations between the bands dominated by Eu  $5d$  and Al  $3p$  orbitals. Given that the itinerant carriers and  $pd$  hybridizations play a crucial role in mediating magnetic interactions, our findings on the band reconstruction across the CDW transition will facilitate the resolving of the mechanism behind chiral spin textures in topological materials with tetragonal lattices. Since the CDW order and the intricate magnetism were also found in several materials with tetragonal lattices, like  $\text{EuGa}_2\text{Al}_2$  [14] and  $\text{GdSb}_x\text{Te}_{2-x-\delta}$  [15,16], we believe that the underlying mechanism in  $\text{EuAl}_4$  is likely to be prevalent across all these materials. Moreover, the observation of a partial CDW gap on the Dirac bands will also stimulate further investigations on the topological properties of  $\text{EuAl}_4$ .

*Acknowledgments.* We thank Artem V. Pronin, Bing Xu, Sheng Li, and Sailong Ju for fruitful discussions, and Gabriele Untereiner for the measurement support. The project was funded by the Deutsche Forschungsgemeinschaft via Grant No. DR228/51-3. Z.W. acknowledges support from the National Natural Science Foundation of China (Grant No. 92065109), the National Key R&D Program of China (Grants No. 2020YFA0308800 and No. 2022YFA1403401), and the Beijing Natural Science Foundation (Grant No. Z190006). Y.-M.D. acknowledges support from the National Natural Science Foundation of China (Grant No. 12174180). R.Y. acknowledges the support from the Alexander von Humboldt Foundation.

P.Z., Z.-W.W. and T.S. grew the single crystals and carried out the transport measurements. Y.-M.D. and R.Y. measured the optical spectroscopy. C.-C.L. performed the first-principles calculations. R.Y. analyzed the data and prepared the manuscript with comments from all authors. R.Y. and M.D. supervised this project.

- [1] N. Nagaosa and Y. Tokura, *Nat. Nanotechnol.* **8**, 899 (2013).
- [2] Q. L. He, T. L. Hughes, N. P. Armitage, Y. Tokura, and K. L. Wang, *Nat. Mater.* **21**, 15 (2022).
- [3] B. A. Bernevig, C. Felser, and H. Beidenkopf, *Nature (London)* **603**, 41 (2022).

- [4] S. Kezilebieke, M. N. Huda, V. Vaňo, M. Aapro, S. C. Ganguli, O. J. Silveira, S. Głodzik, A. S. Foster, T. Ojanen, and P. Liljeroth, *Nature (London)* **588**, 424 (2020).
- [5] W. Shi, B. J. Wieder, H. L. Meyerheim, Y. Sun, Y. Zhang, Y. Li, L. Shen, Y. Qi, L. Yang, J. Jena, P. Werner, K. Koepernik,

- S. Parkin, Y. Chen, C. Felser, B. A. Bernevig, and Z. Wang, *Nat. Phys.* **17**, 381 (2021).
- [6] A. N. Bogdanov and D. A. Yablonskiĭ, *Sov. Phys. JETP* **68**, 101 (1989).
- [7] D. S. Sanchez, G. Chang, I. Belopolski, H. Lu, J. X. Yin, N. Alidoust, X. Xu, T. A. Cochran, X. Zhang, Y. Bian, S. S. Zhang, Y. Y. Liu, J. Ma, G. Bian, H. Lin, S. Y. Xu, S. Jia, and M. Z. Hasan, *Nat. Commun.* **11**, 3356 (2020).
- [8] J. Ma, H. Wang, S. Nie, C. Yi, Y. Xu, H. Li, J. Jandke, W. Wulfhekkel, Y. Huang, D. West, P. Richard, A. Chikina, V. N. Strocov, J. Mesot, H. Weng, S. Zhang, Y. Shi, T. Qian, M. Shi, and H. Ding, *Adv. Mater.* **32**, 1907565 (2020).
- [9] M. Hirschberger, S. Kushwaha, Z. Wang, Q. Gibson, S. Liang, C. A. Belvin, B. A. Bernevig, R. J. Cava, and N. P. Ong, *Nat. Mater.* **15**, 1161 (2016).
- [10] K. Manna, Y. Sun, L. Muechler, J. Kübler, and C. Felser, *Nat. Rev. Mater.* **3**, 244 (2018).
- [11] E. Cheng, W. Xia, X. Shi, H. Fang, C. Wang, C. Xi, S. Xu, D. C. Peets, L. Wang, H. Su, L. Pi, W. Ren, X. Wang, N. Yu, Y. Chen, W. Zhao, Z. Liu, Y. Guo, and S. Li, *Nat. Commun.* **12**, 6970 (2021).
- [12] R. Takagi, N. Matsuyama, V. Ukleev, L. Yu, J. S. White, S. Francoual, J. R. L. Mardegan, S. Hayami, H. Saito, K. Kaneko, K. Ohishi, Y. Onuki, T. H. Arima, Y. Tokura, T. Nakajima, and S. Seki, *Nat. Commun.* **13**, 1472 (2022).
- [13] T. Shang, Y. Xu, D. J. Gawryluk, J. Z. Ma, T. Shiroka, M. Shi, and E. Pomjakushina, *Phys. Rev. B* **103**, L020405 (2021).
- [14] J. M. Moya, S. Lei, E. M. Clements, C. S. Kengle, S. Sun, K. Allen, Q. Li, Y. Y. Peng, A. A. Husain, M. Mitrano, M. J. Krogstad, R. Osborn, A. B. Puthirath, S. Chi, L. Debeer-Schmitt, J. Gaudet, P. Abbamonte, J. W. Lynn, and E. Morosan, *Phys. Rev. Mater.* **6**, 074201 (2022).
- [15] S. Lei, V. Duppl, J. M. Lippmann, J. Nuss, B. V. Lotsch, and L. M. Schoop, *Adv. Quantum Tech.* **2**, 1900045 (2019).
- [16] S. Lei, A. Saltzman, and L. M. Schoop, *Phys. Rev. B* **103**, 134418 (2021).
- [17] Y. Yasui, C. J. Butler, N. D. Khanh, S. Hayami, T. Nomoto, T. Hanaguri, Y. Motome, R. Arita, T. H. Arima, Y. Tokura, and S. Seki, *Nat. Commun.* **11**, 5925 (2020).
- [18] N. D. Khanh, T. Nakajima, X. Yu, S. Gao, K. Shibata, M. Hirschberger, Y. Yamasaki, H. Sagayama, H. Nakao, L. Peng, K. Nakajima, R. Takagi, T.-h. Arima, Y. Tokura, and S. Seki, *Nat. Nanotechnol.* **15**, 444 (2020).
- [19] T. Nomoto, T. Koretsune, and R. Arita, *Phys. Rev. Lett.* **125**, 117204 (2020).
- [20] S. Ramakrishnan, S. R. Kotla, T. Rekiş, J. K. Bao, C. Eisele, L. Noohinejad, M. Tolkiehn, C. Paulmann, B. Singh, R. Verma, B. Bag, R. Kulkarni, A. Thamizhavel, B. Singh, S. Ramakrishnan, and S. van Smaalen, *IUCrJ* **9**, 378 (2022).
- [21] A. Nakamura, T. Uejo, F. Honda, T. Takeuchi, H. Harima, E. Yamamoto, Y. Haga, K. Matsubayashi, Y. Uwatoko, M. Hedo, T. Nakama, and Y. Ōnuki, *J. Phys. Soc. Jpn.* **84**, 124711 (2015).
- [22] M. Stavinoha, J. A. Cooley, S. G. Minasian, T. M. McQueen, S. M. Kauzlarich, C. L. Huang, and E. Morosan, *Phys. Rev. B* **97**, 195146 (2018).
- [23] H. Zhang, X. Y. Zhu, Y. Xu, D. J. Gawryluk, W. Xie, S. L. Ju, M. Shi, T. Shiroka, Q. F. Zhan, E. Pomjakushina, and T. Shang, *J. Phys.: Condens. Matter* **34**, 034005 (2022).
- [24] M. Kobata, S.-i. Fujimori, Y. Takeda, T. Okane, Y. Saitoh, K. Kobayashi, H. Yamagami, A. Nakamura, M. Hedo, T. Nakama, and Y. Ōnuki, *J. Phys. Soc. Jpn.* **85**, 094703 (2016).
- [25] S. Lei, K. Allen, J. Huang, J. M. Moya, T. C. Wu, B. Casas, Y. Zhang, J. S. Oh, M. Hashimoto, D. Lu, J. Denlinger, C. Jozwiak, A. Bostwick, E. Rotenberg, L. Balicas, R. Birgeneau, M. S. Foster, M. Yi, Y. Sun, and E. Morosan, *Nat. Commun.* **14**, 5812 (2023).
- [26] L.-L. Wang, N. K. Nepal, and P. C. Canfield, *arXiv:2306.15068* (2023).
- [27] K. Kaneko, T. Kawasaki, A. Nakamura, K. Munakata, A. Nakao, T. Hanashima, R. Kiyonagi, T. Ohhara, M. Hedo, T. Nakama, and Y. Ōnuki, *J. Phys. Soc. Jpn.* **90**, 064704 (2021).
- [28] M. Dressel and G. Grüner, *Electrodynamics of Solids* (Cambridge University Press, Cambridge, 2002).
- [29] M. Corasaniti, R. Yang, A. Pal, M. Chinotti, L. Degiorgi, A. Wang, and C. Petrovic, *Phys. Rev. B* **100**, 041107(R) (2019).
- [30] Y. Huang, H. P. Wang, W. D. Wang, Y. G. Shi, and N. L. Wang, *Phys. Rev. B* **87**, 100507(R) (2013).
- [31] W. Z. Hu, J. Dong, G. Li, Z. Li, P. Zheng, G. F. Chen, J. L. Luo, and N. L. Wang, *Phys. Rev. Lett.* **101**, 257005 (2008).
- [32] See Supplemental Material at <http://link.aps.org/supplemental/10.1103/PhysRevB.109.L041113> for the sample characterizations and experimental techniques as well as for complementary data and analysis, which include Refs. [5–7,12,14–18,20–23].
- [33] R. Yang, J. W. Huang, N. Zaki, I. Pletikosić, Y. M. Dai, H. Xiao, T. Valla, P. D. Johnson, X. J. Zhou, X. G. Qiu, and C. C. Homes, *Phys. Rev. B* **100**, 235132 (2019).
- [34] E. Uykur, B. R. Ortiz, S. D. Wilson, M. Dressel, and A. A. Tsirlin, *npj Quantum Mater.* **7**, 16 (2022).
- [35] M. Corasaniti, R. Yang, K. Sen, K. Willa, M. Merz, A. A. Haghighirad, M. Le Tacon, and L. Degiorgi, *Phys. Rev. B* **102**, 161109(R) (2020).
- [36] If there is a transfer of SW from high to low energies, the SW ratio will exceed 1 at low energies and then smoothly approach 1 upon increasing  $\omega$  until the full energy scale of the low-energy resonance is reached. If there is a transfer of SW from low to high energies, the SW ratio will fall below 1 until the total energy scale of SW transfer is reached. The latter case suggests some depletion of density of states (DOS), as it would occur when an electronic bands reconstruction happens [29].
- [37] P. E. Jonsson, K. Takenaka, S. Niitaka, T. Sasagawa, S. Sugai, and H. Takagi, *Phys. Rev. Lett.* **99**, 167402 (2007).
- [38] Z. Wang, Y. Su, S.-Z. Lin, and C. D. Batista, *Phys. Rev. B* **103**, 104408 (2021).
- [39] D. N. Basov and T. Timusk, *Rev. Mod. Phys.* **77**, 721 (2005).
- [40] Y. Xu, J. Zhao, C. Yi, Q. Wang, Q. Yin, Y. Wang, X. Hu, L. Wang, E. Liu, G. Xu, L. Lu, A. A. Soluyanov, H. Lei, Y. Shi, J. Luo, and Z.-G. Chen, *Nat. Commun.* **11**, 3985 (2020).
- [41] Z.-G. Chen, L. Wang, Y. Song, X. Lu, H. Luo, C. Zhang, P. Dai, Z. Yin, K. Haule, and G. Kotliar, *Phys. Rev. Lett.* **119**, 096401 (2017).
- [42] In Fig. S2(b) of SM [32], the dip of the MIR absorption in the reflectivity ratio  $R(\omega, 5K)/R(\omega, 150K)$  resides around 0.5 eV; thus we use the data at this point to trace the evolution of the MIR absorptions under magnetic field.
- [43] Eu  $5d$  orbitals mainly hybridize with Al<sub>2</sub> orbital, as Al<sub>2</sub> is closer to Eu atoms, see the inset of Fig. 1(c) and Fig. S5 in SM [32].

- [44] R. Yang, M. Corasaniti, C. C. Le, C. Yue, Z. Hu, J. P. Hu, C. Petrovic, and L. Degiorgi, *npj Quantum Mater.* **7**, 101 (2022).
- [45] The relatively strong correlation effect is estimated in Sec. III of the SM [32].
- [46] S. Araki, Y. Ikeda, T. C. Kobayashi, A. Nakamura, Y. Hiranaka, M. Hedo, T. Nakama, and Y. Ōnuki, *J. Phys. Soc. Jpn.* **83**, 015001 (2014).
- [47] P. W. Anderson, *Phys. Rev.* **79**, 350 (1950).
- [48] J. Kanamori, *J. Phys. Chem. Solids* **10**, 87 (1959).
- [49] J. B. Goodenough, *Phys. Rev.* **100**, 564 (1955).
- [50] H. Ni, W. R. Meier, H. Miao, A. J. May, B. C. Sales, J.-m. Zuo, and M. Chi, [arXiv:2311.17682](https://arxiv.org/abs/2311.17682) (2023).
- [51] X. Y. Zhu, H. Zhang, D. J. Gawryluk, Z. X. Zhen, B. C. Yu, S. L. Ju, W. Xie, D. M. Jiang, W. J. Cheng, Y. Xu, M. Shi, E. Pomjakushina, Q. F. Zhan, T. Shiroka, and T. Shang, *Phys. Rev. B* **105**, 014423 (2022).
- [52] H. Niki, S. Nakamura, N. Higa, M. Yogi, A. Nakamura, K. Niki, T. Maehira, M. Hedo, T. Nakama, and Y. Ōnuki, *JPS Conf. Proc.* **29**, 012007 (2020).
- [53] M. Gen, R. Takagi, Y. Watanabe, S. Kitou, H. Sagayama, N. Matsuyama, Y. Kohama, A. Ikeda, Y. Ōnuki, T. Kurumaji, T.-h. Arima, and S. Seki, *Phys. Rev. B* **107**, L020410 (2023).
- [54] A. Tan, V. Labracherie, N. Kunchur, A. U. B. Wolter, J. Cornejo, J. Dufouleur, B. Büchner, A. Isaeva, and R. Giraud, *Phys. Rev. Lett.* **124**, 197201 (2020).
- [55] J. Gaudet, H.-Y. Yang, S. Baidya, B. Lu, G. Xu, Y. Zhao, J. A. Rodriguez-Rivera, C. M. Hoffmann, D. E. Graf, D. H. Torchinsky, P. Nikolić, D. Vanderbilt, F. Tafti, and C. L. Broholm, *Nat. Mater.* **20**, 1650 (2021).